MSEC2021-1907

RHEOLOGICAL ANALYSIS OF LOW VISCOSITY HYDROGELS FOR 3D BIO-PRINTING PROCESSES

Slesha Tuladhar
Department of Sustainable Product Design and Architecture, Keene State College, Keene, NH.

Cartwright Nelson
Department of Sustainable Product Design and Architecture, Keene State College, Keene, NH.

Md Ahasan Habib, Ph.D.
Department of Sustainable Product Design and Architecture, Keene State College, Keene, NH.

ABSTRACT

Following the success of 3D printing with synthetic polymers like ABS, PLA, Nylon, etc., scientists and researchers have been putting efforts into fabricating bio-compatible materials. It has not only broadened the field of bioengineering and manufacturing but also regenerative medicine. Unlike the traditional 3D printing process, additive bio-manufacturing, also known as 3D bio-printing has a lot of challenges like cell survivability and proliferation, and the mechanical properties of the biomaterials which involve printability and the ability to hold its structural integrity. Proper design of experiments with extensive rheological investigation can help identify useful mechanical property ranges which are directly related to the geometric fidelity of 3D bio-printed scaffolds. Therefore, to investigate the printability of a low viscosity Alginate-Carboxymethyl Cellulose (CMC), multiple concentrations of the mixture were tested maintaining a 8% (w/v) solid content. A set of rheological tests such as the Steady Rate Sweep Test, Three Point Thixotropic Test (3ITT), and Amplitude test were performed. The outcome of those tests showed that the rheological properties can be controlled with the percentage of CMC in the mixtures. The fabricated filaments and scaffolds in the 5 combinations of CMC percentages were analyzed for flowability and shape fidelity. The rheological results and the printability and shape fidelity results were analyzed.

Keywords: Rheology, 3D bio-printing, printability, shape fidelity, shear thinning.

1. INTRODUCTION

Three-dimensional (3D) bio-printing opens a new avenue to fabricate cell encapsulated 3D biomimetic scaffolds for tissue regeneration. A computer-controlled 3D printer is used to extrude cell compatible materials following a layer-by-layer fashion to fabricate user defined 3D scaffold [1-4]. Among various existing 3D bio-printing techniques, extrusion-based bio-printing allows the use of a various range of materials and weight percentages including heterogeneous bio-ink [5, 6]. Hydrogels are demanding candidates for bio-printing because of its bio-compatibility and capacity to arrange 3D environment with a high water content [7].

During hydrogel extrusion, proper rheological properties are required such as flowability through a small nozzle orifice and resisting deformation after release from the nozzle [8]. Immediate deformation after the release of the material with low viscosity can be restricted by developing enough yield strength through quick gelation. The rate of gelation can be controlled by adding a viscosity modifier [9-11], changing temperature [12-14], using an external cross-linker [15, 16], and controlling intrinsic rheological properties of the hydrogels [17, 18]. Normally, in extrusion-based bio-printing, the material is cross-linked after deposition depending on the charges of the scaffold material [19] as depicted in Figure 1.
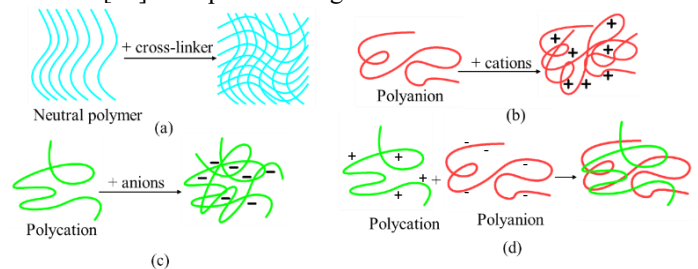

Figure 1: Schematic representation of hydrogel forming mechanism: (a) Chemical hydrogel, (b-c) Ionotropic hydrogel, (d) Co-acervate hydrogel.

However, fabricating 3D structure with hydrogel materials to achieve controlled spatiality is challenging [19]. Various hydrogel materials are mixed to prepare a hybrid hydrogel [20, 21] to achieve the required rheological properties to maintain the filament geometry and eventually the scaffold geometry i.e., the shape fidelity. To achieve the required mechanical strength, viscosity of the hydrogel materials plays an important role as a rheological property [22, 23]. It becomes a conflicting

characteristic when a hydrogel needs to create a comfortable habitant for encapsulated cells during extrusion, and it needs to be highly viscous to maintain the post-printing shape fidelity [24, 25]. For example, hydrogel having lower viscosity i.e., less than 300 centipoise (cps) limits the mechanically stable structure [26]. This mechanical integrity can be increased by improving the viscosity of the hydrogel ($\leq$ 100000 cps). However, it can reduce the cell viability and proliferation [27]. Although in most of the cases, viscosity is interchangeably used as the rheological properties of hydrogel materials, it solely cannot represent the complex rheological behavior of hydrogel materials [18, 28]. In addition to viscosity, two dynamic moduli such as storage modulus (G') and loss modulus (G") are critical [18]. Storage modulus (G') and loss modulus (G") indicate the solid-like and liquid-like characteristics of the hydrogel material, respectively. Identifying the recovery rate of the released hydrogel is important [29] to ensure the shape holding capacity of the fabricated scaffold. In our earlier work, the effect of high viscosity CMC (higher molecular weight) was analyzed in bio-printing process [30]. However, to our best knowledge, the effect of low viscosity CMC on bio-printing process is not reported. In this paper, we will prepare a hybrid hydrogel mixing carboxymethyl cellulose (lower molecular weight) with low viscosity at different weight percentages with alginate maintaining a constant total solid content 8% (w/v) limiting the viscosity range to 300-100000 cps. A set of rheological tests enlisted in Table 2 will be conducted to determine the effect of viscosity modifier on the rheological behavior. Then, the effect of rheological behavior on the printability of the hydrogel materials will be analyzed. Finally, the effect of rheological behavior will be analyzed to determine the shape fidelity of the fabricated scaffold.

2. MATERIALS AND METHODS

2.1 Hybrid hydrogel preparation

Alginate (alginic acid sodium salt from brown algae) and low viscosity carboxymethyl cellulose (CMC) (pH: 6.80) (Sigma-Aldrich, St. Louis, MO, USA) were used as biomaterials to prepare the bio-ink. The chemical formula of those biomaterials is shown in Table 1. Alginate is a common biopolymer. Two monomers such as (1-4)-linked β-Dmannuronic (M) and α-Lguluronic acids (G) form this polymer. Alginate is soluble in the water for having a negatively charged linear copolymer (M and G blocks) chain. It also supports cell growth and exhibits high biocompatibility. The G-block of this material help form gels where GM and M blocks increase the flexibility. Carboxymethylcellulose (CMC) is another naturally or chemically derived anionic water-soluble biopolymer. CMC is a copolymer generated from two monomers, β-D-glucose and β-D-glucopyranose-2-O-(carboxymethyl)-mono-sodium salt. CMC is formed via β-1,4-glucosidic bonds [31]. This material is widely used as thickener [32] which is also non-toxic and non-allergenic in nature. Exiting three hydroxyl groups of each glucose can be substituted by a carboxyl group. Amount of hydroxyl group substituted by

carboxyl group makes the cellulose more soluble, thicken and stable [31]. Various weight percentages of alginate and CMC are used to prepare five different hybrid hydrogel samples maintaining the total solid content 8% (w/v) shown in Table 1. Food colors are used to differentiate the compositions. The overall preparation procedure of hybrid hydrogel is shown in Figure 2.

Table 1: Various Composition prepared with different weight percentages of alginate and CMC.

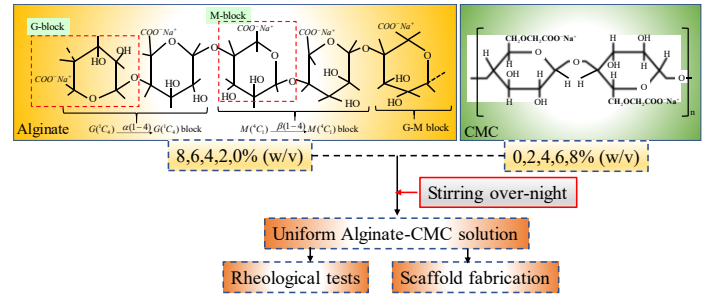| Sample	Alginate (A) (g)	CMC (C) (g)	Alginate/CMC (%)
A_8C_0	8	0	100/0
A_6C_2	6	2	75/25
A_4C_4	4	4	50/50
A_2C_6	2	6	25/75
A_0C_8	0	8	0/100

Figure 2: Preparation of hybrid hydrogel

2.2 Rheological tests

We used a rotational rheometer (MCR 102, Anton Paar, Graz, Austria) with parallel plate geometry (25.0 mm flat plate) to perform the rheological tests. All measurements were recorded with a 1.0 mm plate-plate gap width at room temperature (25°C). We conducted the rheological measurement at room temperature because our extrusion process is performed at room temperature which also facilitate the quick gelation of the deposited filament [24]. A set of rheological tests such as steady rate sweep test, amplitude test, and three-point interval thixotropic test were done. An overview of those tests is shown Table 2.

Table 2: An overview of all rheological tests.

Rheological tests	Variables		Outcome
Steady rate sweep	Shear rate (s^{-1})	0.1 to 100	Flow curve, viscosity, shear stress, shear-thinning behavior
Amplitude sweep	Shear strain (%)	0.1 to 100	Storage modulus (G') and loss modulus (G"), loss tangent (tanδ)
3iTT	Time (s)/Shear rate (s^{-1})	0-60/1 61-65/100 66-185/1	Recovery rate of the hydrogel

By fitting the Power-Law Equation (Equation 1) to the linear region of the shear strain rate vs viscosity plot [33], the shear thinning behavior of the candidate materials will be analyzed in

term of viscosity. The shear thinning co-efficient will be determined using the following equation:

$$\eta = K\dot{\gamma}^{n-1} \qquad (1)$$

Where, η is the viscosity, $\dot{\gamma}$ is the shear rate, and K and n are shear thinning coefficients. While the material is extruded through the nozzle, shear stress occurs throughout the material and is larger along the nozzle wall. The shear thinning behavior of all pseudo-plastic materials can also be approximated by the following Herschel-Bulkley model [34, 35] in term of shear stress:

$$\tau = \tau_0 + K\dot{\gamma}^n \qquad (2)$$

Where, τ and τ_0 are the shear stress and yield stress respectively, K is the consistency index, and n is the flow index. The shear stress at different shear strain will be determined using Equation 2.

2.3 Scaffold fabrication

BioX (CELLINK, Boston, MA), an X-Y-Z-axis 3D bioprinter, is used to extrude hydrogel and fabricate the scaffold. The prepared hybrid hydrogels are loaded into disposal syringes and extruded pneumatically on a stationary build plane. Various printing parameters shown in Table 3 can control the deposition rate of the material. Rhino 6.0 (https://www.rhino3d.com), a Computer-Aided Design (CAD) software is used to design and define the vectorized toolpath of a scaffold. Slicer (https://www.slicer.org), a G-code generator software is used to generate a Bio-X compatible file including the toolpath coordinates and all process parameters to construct the scaffold. We used a layer-upon-layer fashion to deposit materials. The partial physical cross-link of the fabricated scaffold after the print was confirmed by a spray of 4% (w/v) $CaCl_2$. The overall scaffold fabrication process is schematically shown in Figure 3.

Table 3: Process parameters used in this paper

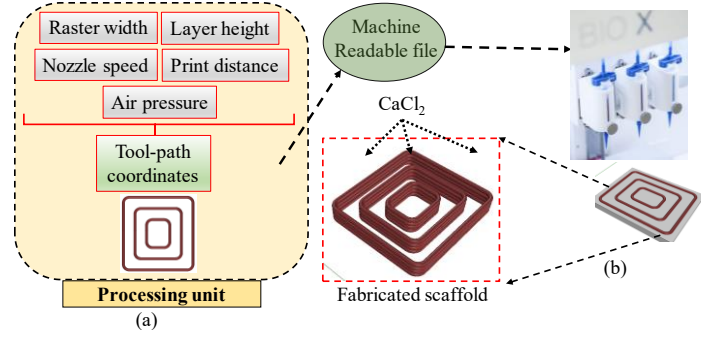| Process parameters	Value/Characteristics
Nozzle diameter	410 μm
Layer height	150 μm
Infill patter	Contour-parallel
Infill density	50%
Print speed	10 mm/s
Air pressure	37 kPa
Print distance	0.405 mm

Figure 3: (a) Preparing machine-readable file, (b) Execution of 3D fabrication.

2.4 Statistics

We presented the data as a form of mean ± standard deviation. A significance level of p = 0.05 with a two-way ANOVA system were used to perform statistical significance of difference of various factors. We used two Statistical software such as Minitab 18.0 and Origin Pro 5.0 to conduct the quantitative and graphical analysis.

3.   RESULTS

3.1 Rheological properties

3.1.1   Shear thinning behavior

Reduction of the viscosity with increasing the shear strain rate on hydrogels i.e., shear-thinning behavior, is crucial for extruding material through a micron-level nozzle [11]. High viscous hydrogel experiences higher shear stress during extrusion through a nozzle, which adversely affect the encapsulated cell. Therefore, the presence of shear thinning behavior of the hydrogel can help create a protective environment for encapsulated cell in extrusion-based 3D bioprinting technique.

Figure 4(a) and 4(b) show the log-log plot of viscosity and shear stress vs shear strain rate respectively. Viscosity decreases with increasing the shear rate whereas the shear stress increases with increasing the shear rate. This phenomenon demonstrates the shear thinning behavior of all the compositions.

Pure 8% alginate showed the lowest viscosity (13430 mPa.S) at 0.1 s^{-1} shear strain. The viscosity increases with increasing the percentage of CMC into the composition. However, at shear strain rate of 0.1 s^{-1}, A_2C_6 showed the highest viscosity (37633 mPa.S). This composition may create the highest number of hydrogen and polar bond due to more easily accessible bond sites of polar carbonyl groups ($C^{\delta+} = O^{\delta-}$) which drives toward a high rate of cross-linking.

The shear thinning coefficients, n and K of Equation 1, were calculated as shown in Table 4 from the regressions of the linear regions of graphs of Figure 4(a). Since, n<1 for all the compositions, it implies that all the compositions have shear thinning behavior. Graph from Figure 4(b) is fitted to the Herschel-Bulkley model with 95% confidence interval to

determine the values of τ_0. All rheological parameters are shown in Table 4.

Table 4: Rheological parameters for various compositions.

Compositions	n	K (mPa.S^n)	τ_0 (Pa)
A_8C_0	0.70	11213.2	7.294712
A_6C_2	0.69	14132.3	8.835086
A_4C_4	0.67	22693.3	2.688427
A_2C_6	0.65	26559.3	6.377949
A_0C_8	0.66	24326.3	0.499546
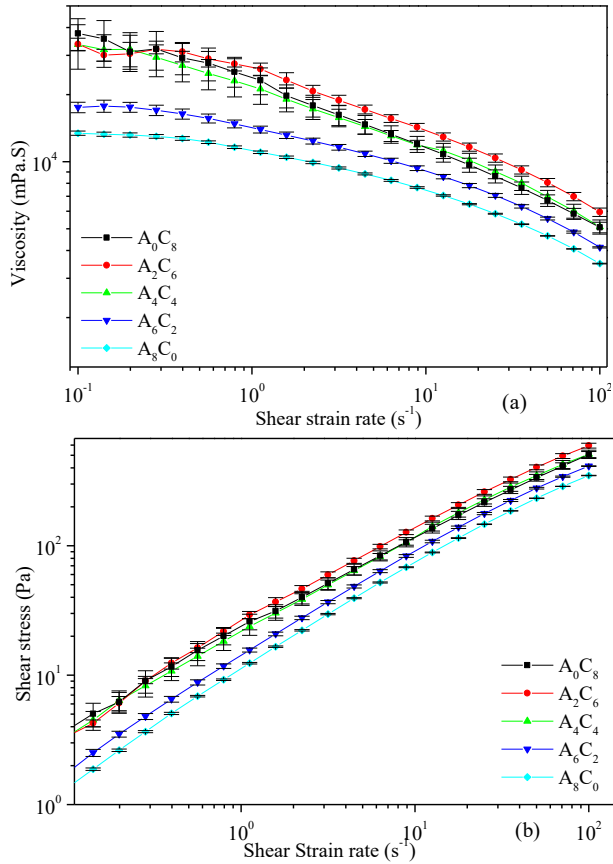
Figure 4: (a) Viscosity with respect to shear strain rate and (b) Shear stress with respect to shear strain rate. These demonstrate all materials have the shear thinning behavior which will help increase the flow through the nozzle.

3.1.2   Storage and loss modulus

One of the characterizing factors for viscoelastic suspension is their complex shear modulus (G*) which is expressed by the following equation:

$$G^* = G' + iG'' \qquad (4)$$

Where, G' is the elastic (or storage) modulus, the real component. This reflects the solid-like character of the hydrogel. G'' is viscous (or loss) modulus, the imaginary component of Equation (4) which reflects the liquid-like character of the hydrogel. The amplitude test for various compositions of the hydrogels at 1 Hz represented the outcome of G' and G'' vs shear strain (%) in Figure 5.

It is clear from Figure 5 that with increasing the percentage of CMC into the alginate suspension, the physical state of the hydrogel is changing from a liquid-like to a solid-like state. Since, the loss modulus dominates the storage modulus in all compositions; the liquid-like state was dominating for all compositions. To provide more insight into solid and liquid-like behavior of hydrogels, the dynamic mechanical loss tangent ($tan\delta = G''/G'$) was determined as shown in Figure 5. Tangent value smaller than 1 predominantly reflects the elastic behavior, and greater than 1 predominantly indicates viscous behavior. It is clear from the Figure 5 that the difference between G" and G' was reduced with increasing the weight percentage of CMC in the composition. Therefore, the $tan\delta$ value increased from 2.23 to 2.62 at 1% shear strain with reducing the percentage of CMC as shown in Figure 5. The $tan\delta$ value increased with increasing the shear strain, which indicates the dominance of liquid-like state over solid-state. Loss tangent at different shear strain will help achieve or control the solid-like state of the bio-ink at lower strain (<0.1%). Therefore, it can be concluded that with less shear strain, G' may dominate which will help maintain the shape holding capacity of the fabricated scaffold with compositions having more content weight of CMC. Bio-printing with less pressure will also minimize the cell death in the post-printing period and eventually increase cell viability in long incubation period [24, 36].
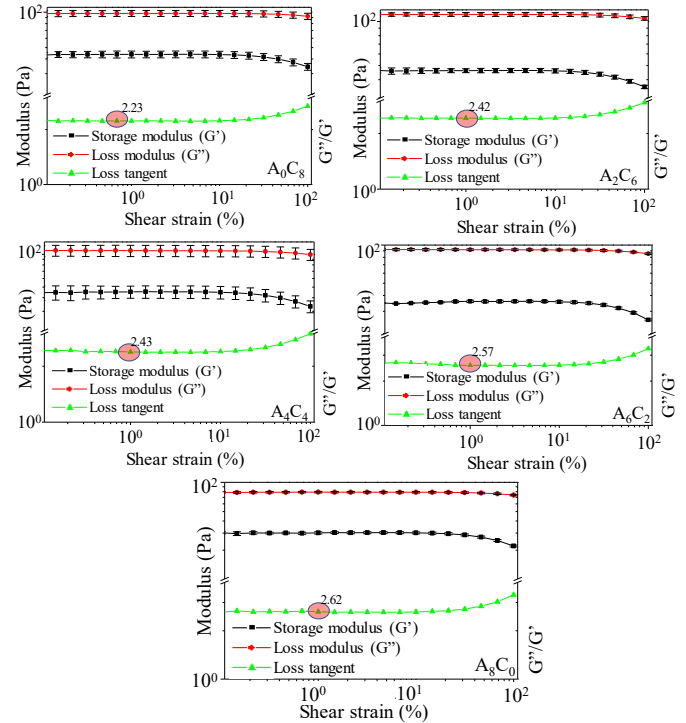

Figure 5: Storage modulus (solid-like), loss modulus (liquid-like), and loss tangent (loss/storage) of various compositions.

3.1.3　Hydrogel recovery rate

Three point-interval-thixotropy-tests were conducted on all the compositions to determine the recovery rate after extruding the hydrogels. This information is critical before starting the printing because, it is directly related to the shape fidelity of the filament. In this test, the first interval imitates the at-rest state of sample, the second interval resembles the hydrogel decomposition under high shear i.e. hydrogel experiences high shear during extrusion, and third interval reflects the structure retention after hydrogel extrusion as shown in Figure 6.

In the first interval, a shear rate of 1.0 s^{-1} was applied for 60 seconds. After that the shear rate was increased to 100 s^{-1} for 5 seconds. Finally, shear rate was reduced to 1.0 s^{-1} and held for 120 seconds. Figure 6 shows that the recovery rate of A_2C_6 was 87% of its viscosity after 60 seconds where the recovery rate increased to 90% after 120 seconds. Therefore, it is a good indication that the deposited filament will hold its shape and maintain the geometric fidelity. The recovery rates of A_0C_8, A_4C_4, A_6C_2, and A_0C_8 after 60s and 120s are shown in Table 5. A_6C_2 and A_0C_8 were showing very promising recovery rate. Therefore, it should also show a good shape fidelity after deposition.

A shear rate of 100 s^{-1} was applied on the at-rest hydrogel after 60s which breaks down the initial network structures of the hydrogel and demonstrated a spike of shear stress at 61s shown in Figure 6(b). After the hydrogel is extruded through the nozzle at a certain shear rate, it takes time to recover the internal network. In most cases, when the shear is released, a portion of the bond remains irrecoverable. Therefore, when the shear rate was reduced to 1.0 s^{-1} from 100 s^{-1}, the amount of shear stress for all the compositions were lower than the initial stage of the tests.
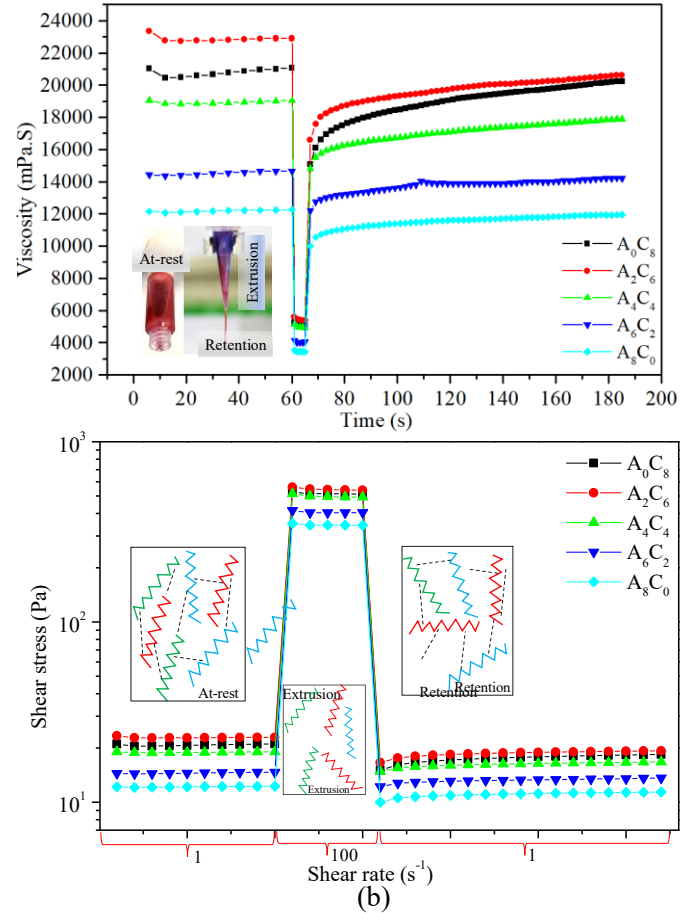

Figure 6: Three-point thixotropic test data analyzed two ways: (a) Viscosity vs time and (b) shear stress vs shear rate.

Table 5: Recovery rate of various compositions at 60s and 120s.

Compositions	Viscosity (mPa.S) after at 60s	Viscosity (mPa.S) after at 125s	Viscosity (mPa.S) after at 185s	Recovery rate (%) after 60s	Recovery rate (%) after 120s
A_0C_8	21057	19201	20245	91.2	96.1
A_2C_6	22902	19846	20634	86.6	90.1
A_4C_4	19033	17174	17881	90.2	93.9
A_6C_2	14653	13889	14221	94.8	97.0
A_8C_0	12267	11632	11958	94.8	97.5

3.2 Printability and shape fidelity

Acellular filaments were deposited with the compositions of A_0C_8, A_2C_6, A_4C_4, A_6C_2, and A_8C_0 for investigating their manufacturability or printability. The images of fabricated filaments are captured using the CK Olympus bright field microscope (Tokyo, Japan). The width of the filament is determined using ImageJ. Fabricated scaffolds (8.5mm × 8.5 mm) and corresponding filaments with their width are shown Figure 7. This figure indicates that by increasing the solid content of CMC in the composition, the diffusion of the filament decreased, i.e. properly holding the geometry of the filament, which eventually will improve the overall shape fidelity of the fabricated scaffold. However, due to higher recovery rate, A_8C_0

shows a deviation from this trend. Filament fabricated with the composition of A_2C_6 showed better shape holding ability. Filaments fabricated with A_4C_4 and A_6C_2 showed 48% and 77% more diffusion than filament fabricated with A_2C_6. Figure 7 also represents the crosslinked scaffolds and filaments. Scaffolds fabricated with A_0C_8 composition almost dissolved into $CaCl_2$ due to the absence of alginate.
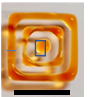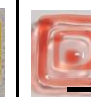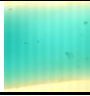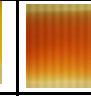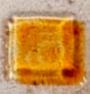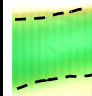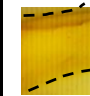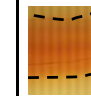
	A_0C_8	A_2C_6	A_4C_4	A_6C_2	A_8C_0
Scaffold					
Filament					
Filament Width (µm)	719 ± 90	731 ± 71	1081 ± 34	1294 ± 57	739 ± 88
Crosslinked Scaffold					
Crosslinked Filament					

Figure 7: Scaffolds and filaments fabricated with various compositions. Bar = 5 mm.

4. DISCUSSION

Various efforts have been reported to mix multiple hydrogel materials to achieve the proper rheological properties and help print the scaffolds to maintain the shape fidelity [29, 37]. In our earlier work, we used high viscosity CMC in alginate to analyze printability, shape fidelity and cell viability [30]. However, according to our best knowledge , the effect of low viscosity CMC on the bio-printing process is not reported. In this paper, we prepared a hybrid hydrogel mixing carboxymethyl cellulose (lower molecular weight) with low viscosity at different weight percentages with alginate maintaining a constant total solid content 8% (w/v). The highest viscosity we achieved is 37633 cps for A_2C_6 which is within the limit of 300-100000 cps. A set of rheological tests was conducted to determine the effect of low viscosity CMC on the hybrid hydrogels in term of viscosity, shear stress, storage modulus, loss modulus, and recovery rate. The relationship between the printability and rheological properties of the compositions were identified. This study identified that compositions A_2C_6 having higher viscosity at lower shear rate and higher post-printing recovery rate can create filament with proper shape fidelity. Since pure alginate helps a little to create cell attachment sites in the scaffold due to the lack of bioligands necessary for the mammalian cell adhesion [38, 39] in incubation period, the addition of low viscosity CMC can help to improve the cell attachment and overall cell viability in long run.

Since, hydrogel with lower viscosity can better assist the cell proliferation [27], it is our expectation that this composition will show better cell viability in incubation period. The future direction of this research is to identify the maximum height of the scaffolds that compositions A_2C_6 and A_4C_4 can fabricate while ensuring shape fidelity. Moreover, the scaffolds will be fabricated with A_2C_6 and A_4C_4 compositions encapsulating cells and analyzed for cell viability and proliferation.

5. CONCLUSION

In this research, we did a rheological analysis of various compositions prepared with alginate and low viscosity CMC maintaining a solid content of 8%. We determined the effect of low viscosity CMC on the hybrid hydrogels in term of viscosity, shear stress, storage modulus, loss modulus, and recovery rate. The relationship between the printability and rheological properties of the compositions were identified. The illustrated rheological tests and corresponding printability of those compositions can help direct the 3D bio-fabrication of the controlled geometries of the scaffold scaffolds, which will contribute in future efforts to fabricate functional tissues.

REFERENCES

1. Murphy, S.V. and A. Atala, *3D bioprinting of tissues and organs.* Nature biotechnology, 2014. **32**(8): p. 773-785.
2. Jia, W., et al., *Direct 3D bioprinting of perfusable vascular constructs using a blend bioink.* Biomaterials, 2016. **106**: p. 58-68.
3. Axpe, E. and M.L. Oyen, *Applications of alginate-based bioinks in 3D bioprinting.* International Journal of Molecular Sciences, 2016. **17**(12): p. 1976.
4. Skardal, A. and A. Atala, *Biomaterials for integration with 3-D bioprinting.* Annals of biomedical engineering, 2015. **43**(3): p. 730-746.
5. Ozbolat, I.T. and M. Hospodiuk, *Current advances and future perspectives in extrusion-based bioprinting.* Biomaterials, 2016. **76**: p. 321-343.
6. Wang, L.L., et al., *3D extrusion bioprinting of single- and double-network hydrogels containing dynamic covalent crosslinks.* Journal of Biomedical Materials Research Part A, 2018.
7. Malda, J., et al., *25th anniversary article: engineering hydrogels for biofabrication.* Advanced materials, 2013. **25**(36): p. 5011-5028.
8. M'barki, A., L. Bocquet, and A. Stevenson, *Linking Rheology and Printability for Dense and Strong*

Ceramics by Direct Ink Writing. Scientific Reports, 2017. **7**(1): p. 6017.

9. Ahlfeld, T., et al., *A methylcellulose hydrogel as support for 3D plotting of complex shaped calcium phosphate scaffolds.* Gels, 2018. **4**(3): p. 68.

10. Jin, Y., et al., *Self-Supporting Nanoclay as Internal Scaffold Material for Direct Printing of Soft Hydrogel Composite Structures in Air.* ACS Applied Materials & Interfaces, 2017. **9**(20): p. 17456-17465.

11. Li, H., et al., *3D bioprinting of highly thixotropic alginate/methylcellulose hydrogel with strong interface bonding.* ACS applied materials & interfaces, 2017. **9**(23): p. 20086-20097.

12. Ahn, G., et al., *Precise stacking of decellularized extracellular matrix based 3D cell-laden constructs by a 3D cell printing system equipped with heating modules.* Scientific Reports, 2017. **7**(1): p. 8624.

13. Di Giuseppe, M., et al., *Mechanical behaviour of alginate-gelatin hydrogels for 3D bioprinting.* Journal of the mechanical behavior of biomedical materials, 2018. **79**: p. 150-157.

14. Mouser, V.H., et al., *Yield stress determines bioprintability of hydrogels based on gelatin-methacryloyl and gellan gum for cartilage bioprinting.* Biofabrication, 2016. **8**(3): p. 035003.

15. Tabriz, A.G., et al., *Three-dimensional bioprinting of complex cell laden alginate hydrogel structures.* Biofabrication, 2015. **7**(4): p. 045012.

16. Kuo, C., et al., *Printability of Hydrogel Composites Using Extrusion-Based 3D Printing and Post-Processing with Calcium Chloride.* J Food Sci Nutr, 2019. **5**: p. 051.

17. Kiyotake, E.A., et al., *Development and quantitative characterization of the precursor rheology of hyaluronic acid hydrogels for bioprinting.* Acta biomaterialia, 2019.

18. Gao, T., et al., *Optimization of gelatin–alginate composite bioink printability using rheological parameters: a systematic approach.* Biofabrication, 2018. **10**(3): p. 034106.

19. Kirchmajer, D.M. and R. Gorkin Iii, *An overview of the suitability of hydrogel-forming polymers for extrusion-based 3D-printing.* Journal of Materials Chemistry B, 2015. **3**(20): p. 4105-4117.

20. Chen, Y., et al., *3D Bioprinting of shear-thinning hybrid bioinks with excellent bioactivity derived from gellan/alginate and thixotropic magnesium phosphate-based gels.* Journal of Materials Chemistry B, 2020.

21. Yu, F., et al., *Evaluation of a polyvinyl alcohol-alginate based hydrogel for precise 3D bioprinting.* Journal of Biomedical Materials Research Part A, 2018. **106**(11): p. 2944-2954.

22. Colosi, C., et al., *Microfluidic Bioprinting of Heterogeneous 3D Tissue Constructs Using Low-Viscosity Bioink.* Advanced Materials, 2016. **28**(4): p. 677-684.

23. Therriault, D., S.R. White, and J.A. Lewis, *Rheological behavior of fugitive organic inks for direct-write assembly.* Applied Rheology, 2007. **17**(1): p. 10112-11411.

24. Ouyang, L., et al., *Effect of bioink properties on printability and cell viability for 3D bioplotting of embryonic stem cells.* Biofabrication, 2016. **8**(3): p. 035020.

25. Blaeser, A., et al., *Controlling shear stress in 3D bioprinting is a key factor to balance printing resolution and stem cell integrity.* Advanced healthcare materials, 2016. **5**(3): p. 326-333.

26. He, Y., et al., *Research on the printability of hydrogels in 3D bioprinting.* Scientific reports, 2016. **6**: p. 29977.

27. Khalil, S. and W. Sun, *Bioprinting endothelial cells with alginate for 3D tissue constructs.* Journal of biomechanical engineering, 2009. **131**(11): p. 111002.

28. Göhl, J., et al., *Simulations of 3D bioprinting: predicting bioprintability of nanofibrillar inks.* Biofabrication, 2018. **10**(3): p. 034105.

29. Jiang, Y., et al., *Rheological behavior, 3D printability and the formation of scaffolds with cellulose nanocrystals/gelatin hydrogels.* Journal of Materials Science, 2020. **55**(33): p. 15709-15725.

30. Habib, A., et al., *3D printability of alginate-carboxymethyl cellulose hydrogel.* Materials, 2018. **11**(3): p. 454.

31. Han, Y. and L. Wang, *Sodium alginate/carboxymethyl cellulose films containing pyrogallic acid: physical and antibacterial properties.* Journal of the Science of Food and Agriculture, 2017. **97**(4): p. 1295-1301.

32. Tongdeesoontorn, W., et al., *Effect of carboxymethyl cellulose concentration on physical properties of biodegradable cassava starch-based films.* Chemistry Central Journal, 2011. **5**(1): p. 6.

33. Therriault, D., S.R. White, and J.A. Lewis, *Rheological behavior of fugitive organic inks for direct-write assembly.* Applied Rheology, 2007. **17**(1): p. 10112-1-10112-8.

34. Shao, Y., et al., *Use of microfibrillated cellulose/lignosulfonate blends as carbon precursors: Impact of hydrogel rheology on 3D printing.* Industrial & Engineering Chemistry Research, 2015. **54**(43): p. 10575-10582.

35. Costakis Jr, W.J., et al., *Additive manufacturing of boron carbide via continuous filament direct ink writing of aqueous ceramic suspensions.* Journal of the European Ceramic Society, 2016. **36**(14): p. 3249-3256.

36. Chang, R., J. Nam, and W. Sun, *Effects of dispensing pressure and nozzle diameter on cell survival from solid freeform fabrication–based direct cell writing.* Tissue Engineering Part A, 2008. **14**(1): p. 41-48.

37. Ahlfeld, T., et al., *Development of a clay based bioink for 3D cell printing for skeletal application.* Biofabrication, 2017. **9**(3): p. 034103.

38.   Sun, J. and H. Tan, *Alginate-based biomaterials for regenerative medicine applications.* Materials, 2013. **6**(4): p. 1285-1309.

39.   Lee, K.Y. and D.J. Mooney, *Alginate: properties and biomedical applications.* Progress in polymer science, 2012. **37**(1): p. 106-126.